Quignon, B., Pilkington, G. A., Thormann, E., Claesson, P., Ashfold, M. N. R., Mattia, D., ... Briscoe, W. H. (2013). Sustained Frictional Instabilities on Nanodomed Surfaces:: Stick-Slip Amplitude Coefficient. ACS Nano, 7(12), 10850–10862. 10.1021/nn404276p

Sustained Frictional Instabilities on Nanodomed Surfaces: *Stick-Slip Amplitude Coefficient*

Benoit Quignon,[†] Georgia A. Pilkington,[†] Esben Thormann,[‡,§] Per M. Claesson,[‡] Michael N.R. Ashfold,[†] Davide Mattia,[¶] Hannah Leese,[¶,∥] Sean A. Davis,[†] and Wuge H. Briscoe[*,†]

School of Chemistry, University of Bristol, Cantock's Close, Bristol BS8 1TS, UK, Royal Institute of Technology (KTH), Drottning Kristinas Väg 51, SE-100 44 Stockholm, Sweden, and Department of Chemical Engineering, University of Bath, Bath BA2 7AY, UK

E-mail: wuge.briscoe@bristol.ac.uk

Abstract

Understanding the frictional properties of nanostructured surfaces is important due to their increasing application in modern miniaturised devices. In this work, lateral force microscopy was used to study the frictional properties between an AFM nanotip and surfaces bearing well-defined nanodomes comprising densely packed prolate spheroids, of diameters ranging from tens to hundreds of nanometres. Our results show that the average lateral force varied linearly with applied load, as described by Amontons' first law of friction, although no direct correlation between the sample topographic

[*]To whom correspondence should be addressed
[†]School of Chemistry, University of Bristol
[‡]Surface and Corrosion Science, Department of Chemistry, Royal Institute of Technology (KTH)
[¶]Department of Chemical Engineering, University of Bath
[§]Current address: Department of Chemistry, Technical University of Denmark, Kemitorvet 206, DK-2800 Kgs. Lyngby, Denmark
[∥]Current address: Department of Chemistry, South Kensington Campus, Imperial College London, London SW7 2AZ, UK

properties and their measured friction coefficients was identified. Furthermore, all the nanodomed textures exhibited pronounced oscillations in the shear traces, similar to the classic stick-slip behaviour, under all the shear velocities and load regimes studied. That is, the nanotextured topography led to sustained frictional instabilities, effectively with no contact frictional sliding. The amplitude of the stick-slip oscillations, σ_f, was found to correlate with the topographic properties of the surfaces, and scale linearly with the applied load. In line with the friction coefficient, we define the slope of this linear plot as the *stick-slip amplitude coefficient* (*SSAC*). We suggest that such stick-slip behaviours are characteristics of surfaces with nanotextures, and that such local frictional instabilities have important implications to surface damage and wear. We thus propose that the shear characteristics of the nanodomed surfaces can not be fully described by the framework of Amontons' laws of friction, and that additional parameters (*e.g.* σ_f and SSAC) are required, when their friction, lubrication and wear properties are important considerations in related nanodevices.

Keywords: Friction, Amontons' laws, Stick-slip, nano-textured surfaces, nanostructured surfaces, nanodomes, nanotribology.

As the dimensions of modern devices miniaturise, the surface-to-volume ratio in the system increases concurrently, and consequently surface-related issues such as friction, adhesion and stiction become increasingly important.[1–6] Recent advances in nanopatterning techniques such as template printing, spin coating, nanolithography,[7] ion beam lithography[8] and micromachining[9] have facilitated ready implementation of nano- to micro-sized surface patterns in modern devices for enhanced or additional performance and functionalities, for example in applications such as gas sensors, batteries and magnetic storage.[10] Therefore, understanding the tribological properties of surfaces with well-defined nanotextures is relevant to these modern applications.

Although it is reported that the frictional behaviour of textured surfaces is generally different compared to smooth surfaces, a clear understanding of the mechanisms underlying friction and wear of surfaces bearing *nanotextures* is yet to be fully established.[11] Many

friction studies have focused on testing the validity and applicability of Amonton's laws, that is, how the frictional force f_s depends on the applied load, the sliding velocity and the contact area. However, despite it being widely accepted that surface roughness greatly influences tribological behaviour, a unified relationship between roughness, friction and adhesion at the nanoscale is yet to emerge.

Over the past decade, a number of friction studies have been carried out on surfaces with well-defined topographies. Ando *et al.*[12,13] made atomic force microscope (AFM) adhesion and friction measurements on surfaces with spherical asperities of various radii of curvature, created by focused ion beam lithography, against a square tip of 0.49 µm^2 in area, and found that the friction force decreased as the groove depth of the asperities and sliding speed increased. The same conclusions were reached by Mo *et al.*[14] using a conventional AFM tip sliding across a surface patterned with gold nanopillars of 20 mm in height and 2 µm in diameter. Yoon *et al.*[15] investigated the frictional behaviour of a silicon surface patterned with cone-shaped poly(methyl methacrylate) pillars of 500 nm in height, and with a pillar diameter of 50 nm at the top and 150 nm at the bottom, against a borosilicate glass sphere of 1.25 µm in diameter attached to an AFM tip. They recorded a smaller friction coefficient on the patterned surfaces than on flat silicon, and attributed it to a reduction in the area of contact. In addition, the longer pillars exhibited a higher friction coefficient than the shorter ones, as the longer pillars underwent more elastic deformation which led to an increase in the contact area. Thormann *et al.* studied friction between 7 and 32 µm silica micro-particles against silicon needles of 3 µm in length spaced 1.4 µm apart, and concluded that the friction coefficient was independent of the apparent number of contact points and the sliding velocity.[16] Using a tribometer, Zou *et al.* reported a significant decrease in friction and adhesion on a silicon surface sparsely textured with 200 nm nanoparticles, against a large spherical tip of 100 µm in radius, which was again attributed to a decrease of the real area of contact as compared to a flat surface.[17] Conversely, Choi *et al.* reported a non-linear increase of friction between porous anodic alumina films of

increasing porosity and an increase of the friction coefficient compared to flat aluminium, when measured using an AFM mounted with tips of 930 nm and 2280 nm in radius. This was attributed to the increased contribution of the contact with adjacent surface features as well as the decreased stiffness of the porous material.[18] More recently, Pilkington *et al.* studied the frictional behaviour of several different surfaces bearing nanodomes, nanorods, nanograins and nanodiamonds against both modified and unmodified AFM tips.[19] They reported a linear increase of friction with the applied load and noticed a weak velocity dependence. Furthermore, they found that the frictional traces exhibited large oscillation, *i.e.* peaks and troughs, whose magnitude and density depended upon the topographical nature of the nanotextured surfaces. From these conclusions, it seems important to consider the shear characteristics, *i.e.* the transient behaviour of the lateral force as a function of time, as well as the load and velocity dependence of friction, in order to fully characterise the frictional properties of such nanotextured surfaces.

The oscillations in the shear traces observed by Pilkington *et al.*[19] are similar to the stick-slip behaviour between two sliding surfaces under certain conditions. Stick-slip motion can be found at all length scales, ranging from the atomic scale up to the macroscale where stick-slip is responsible for common-life phenomena such as the noise of squeaking doors and car brakes' squeal.[20] Furthermore, natural phenomena such as earthquakes have also been recognised as being the result of stick-slip frictional instabilities of rocks.[21] At the microscale level, the deformation of asperities under stress needs to be taken into consideration. Thus, the rate of deformation and the increase of the contact area caused by the creep of the contacting asperities as well as ageing effects are important factors.

Macroscopically, stick-slip behaviour is defined as a period of long stick followed by rapid sliding of the contacting surfaces, with the static friction coefficient μ_s depending on the mating time of the surfaces. For instance, its magnitude has been found to grow logarithmically with the sliding velocity[22–24] in a humid environment[25] as the contact area increased with time due to asperities' creep. This phenomenon is commonly described using

rate and state-dependent laws such as the *Dieterich-Ruina law*.[26,27] Recently, an analogy between this phenomenon and interfacial bonding has been made in a rate and state friction experiment between silica surfaces in slide-hold-slide experiments employing AFM. [28]

Many models have been developed in order to understand and explain the effects of stick-slip at the nanoscale, relating it to parameters such as the mechanical and the molecular properties of the interacting bodies. For instance, the *surface topology model* relates the stick-slip amplitude and frequency to both roughness and mechanical properties of the rubbing materials. Whereas *rate and state models* have been used to describe the freeze-melting transition cycles in the case of lubricated systems studied with the surface force apparatus (SFA).[29] The *Prandtl-Tomlinson* model is frequently used to describe stick-slip motion [30,31] which is particularly relevant to AFM measurements. In this simple model, the AFM tip, represented by a point mass elastically coupled to a sliding mass, interacts with a periodic sinusoidal potential. Under certain conditions, the tip gets stuck in a potential minimum until it acquires enough potential energy to "climb up" the potential hill, before getting stuck again at the next minimum. The cycle then repeats again, thus producing the characteristic saw-tooth pattern in the shear trace, evocative of the unstable sliding motion of the tip on the surface. Although the *Prandtl-Tomlinson model*, due to its simplistic nature, is not able to describe all the characteristics of a real tribological system, it remains widely used and provides accurate correlations with AFM experiments on various atomically flat surfaces. [32,33] It is also able to describe many useful properties of dry friction, for instance the influence of system parameters such as stiffness as well as the potential amplitude and periodicity on the transition between stick-slip and continuous friction regimes. [31] The use of an interaction potential, however, implies that important information regarding both the properties of the tip (*e.g.* material properties, radius of curvature) and the contact surfaces (*e.g.* topography) are explicitly considered. [34]

However, the stick-slip behaviour and mechanisms involving nanotextured surfaces are not particularly well studied, where both the macroscopic material properties and the well-

defined topography of nanotextures are expected to make convoluted contributions to the overall frictional behaviour of these surfaces. Here, we report the stick-slip frictional behaviour of nanodomed-textured surfaces with varying topographic features measured by friction force microscopy. Our results will provide an insight towards the stick-slip mechanisms involved on surfaces with well-defined nanotextures which are increasingly encountered in modern device design. Although numerous previous studies have focused on the friction and adhesion behaviour of nanostructured surfaces, few have taken into consideration the sustained frictional instabilities that are induced by the presence of nanotextures on surfaces, which may have important implications to the wear characteristics of such surfaces.

Results and Discussion

Characterisation of nanodomes

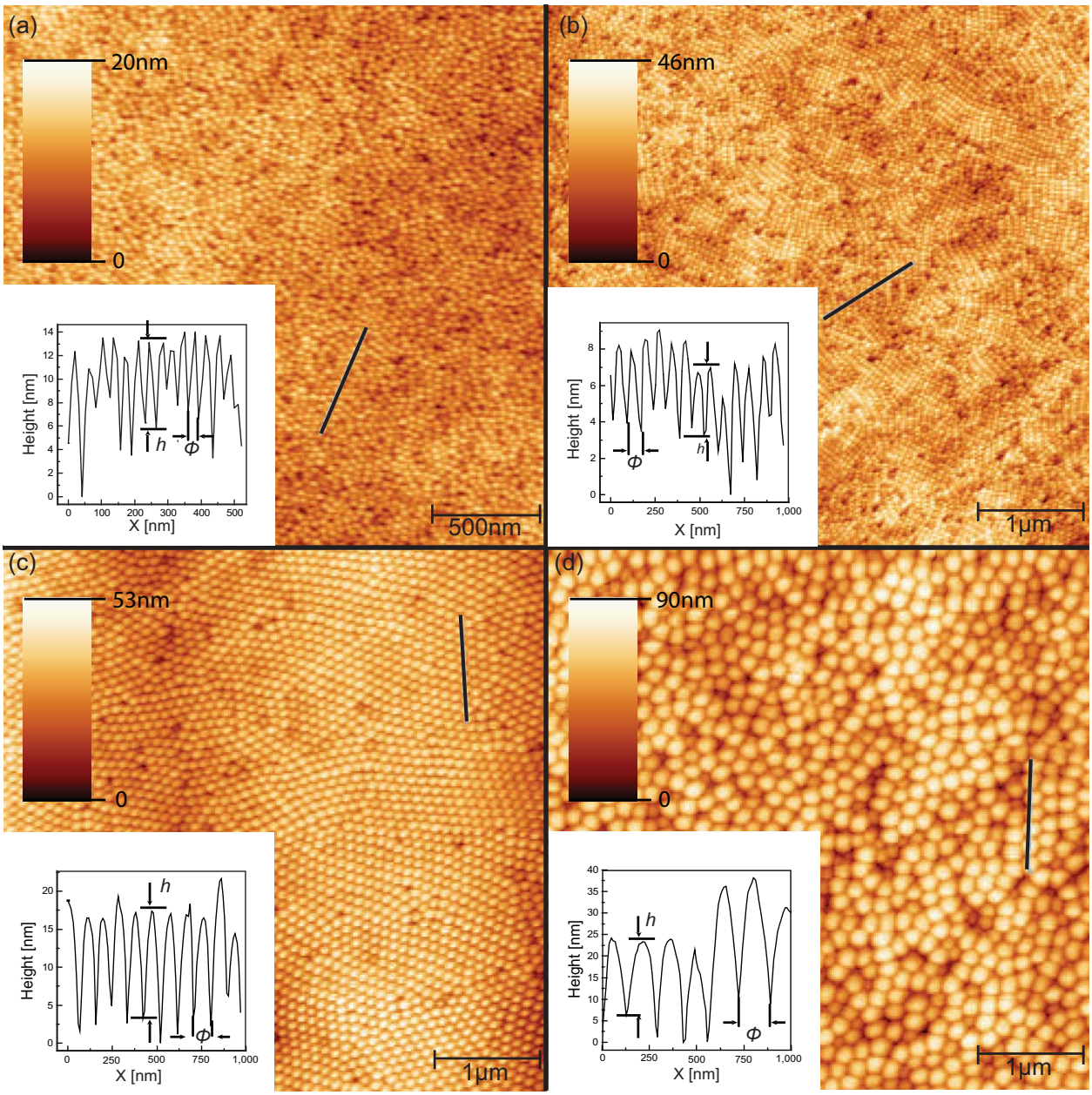

Figure 1: AFM micrographs of nanodomed-textured samples with an average dome diameter of (a) to (d) $\phi = 35, 64, 92$ and $157\,\mathrm{nm}$, respectively. A line profile, corresponding to the black line, is shown on the inset in each figure, revealing the profile of individual domes.

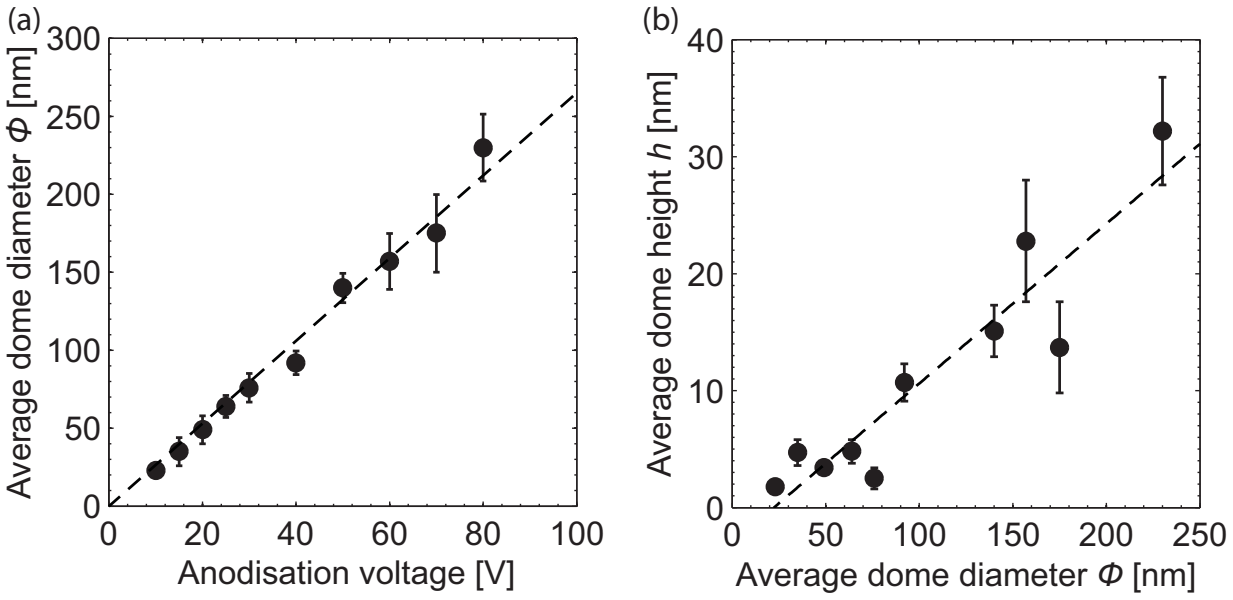

Figure 2: (a) Nanodome diameter ϕ *vs.* the anodisation voltage, and (b) average dome height h *vs.* average dome diameter ϕ.

In order to characterise the topography of the nanodomed-surfaces, the samples were imaged by tapping mode AFM. For image analysis, a first order levelling was applied prior to the calculation of the topography parameters and the surface height minima were set to 0 nm. Densely-packed nanodomes were found on the surface, whose topographic properties (*i.e.* dome diameter ϕ, mean roughness R_a, r.m.s. roughness R_q and dome height h) varied depending on the anodisation voltage applied during the preparation process. In line with previous reports,[35,36] and as seen in the line profile insets in Figure 1, the domes had a prolate spheroid shape, whose diameter ϕ varied from 23 nm to 230 nm, and a height h calculated using topographic line profiles ranging from 1.8 nm to 32 nm. Detailed sample characteristics can be found in Table S1. A 2D FFT of the images (*cf.* Figure S3) did not reveal the presence of any long range order. The diameter ϕ of the domes obtained varied approximately linearly with the anodisation voltage as shown in Figure 2(a), and the correlation between other topographical parameters and the dome diameter was less clear-cut. However, a general trend of increasing dome height was observed with the increasing dome diameter (*cf.* Figure 2(b)). Our friction measurements were performed between a

nano-sized AFM tip of 20 nm nominal radius and 20 nm height and these textured surfaces bearing densely packed prolate spheroid nanodomes of different dimensions and of different nano-roughness.

Friction signal characteristics

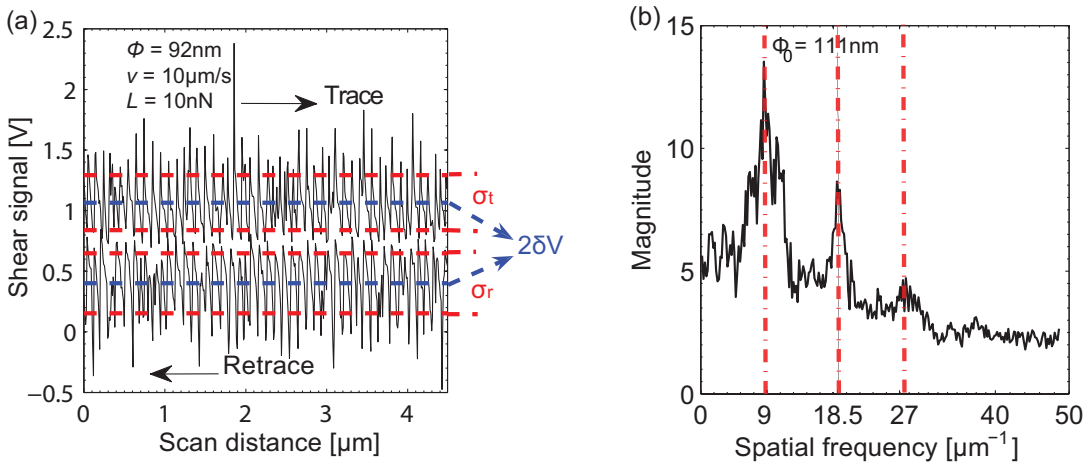

Figure 3: (a) A typical friction shear trace obtained on samples bearing nanodome textures. This profile is obtained on a surface bearing nanodomes of $\phi = 92\,\mathrm{nm}$ at a $v = 10\,\mu\mathrm{m\,s^{-1}}$ velocity under an applied load of $L = 10\,\mathrm{nN}$. The blue lines correspond to the averages for the trace (upper) and retrace (lower) in the friction loop. The red lines denote how the standard deviations from the mean are defined for the trace (σ_t) and retrace (σ_r); (b) 1D Fourier transform of the friction trace presented in (a), revealing three peaks. The first peak represents the spatial frequency corresponding a dome diameter of $\phi_0 = 111\,\mathrm{nm}$, the two other peaks being higher harmonics.

First, it should be noted that the friction force is defined here as the average lateral force experienced by the tip. The shear trace profiles obtained are dominated by sharp, recurring peaks for all the nanodome samples at all the load and shear velocities examined. Examples of raw shear traces is shown in Figure 3, with further examples given in Figure S2. The presence of such characteristics has previously been reported in the literature on a wide range of nanostructured surfaces.[19] Weilandt *et al.* studied friction at an highly orientated pyrolite graphite (HOPG) surface in a $NaClO_4$ electrolyte medium liquid and observed friction peaks corresponding to HOPG steps whilst scanning the step upwards and downwards. They

attributed the friction peaks to both topographic and frictional contributions.[37] A similar conclusion was also reached by Müller *et al.*,[38] who reported the presence of frictional peaks on HOPG under high vacuum, which were attributed to both topographic and electronic effects. Topographic-induced peaks were also reported on AgBr crystals and Ag_0 crystallite surface steps,[39] resulting from the additional torque experienced by the tip on sudden surface elevations given by:

$$\tau \approx Ls\left(\mu + \frac{dz}{dx}\right) \tag{1}$$

where L is the external load, s is the distance between the tip vertex and the contact point and dz/dx is the first derivative of the surface height at the point of contact. Using grooved-silicon samples of varying groove depths (35 and 160 nm), Sung *et al.*[40] reported that the magnitude of the local surface slope greatly affected the variation of the friction force encountered, and that the lateral force decreased for negative slope changes and increased for positive slope changes. This is in contradiction with the macroscopic *Ratchet mechanism*, which states that the change in friction is related solely to the nature of the slope itself,[41] giving rise to a coefficient of friction described by:

$$\mu = \mu_0 + tan\theta \tag{2}$$

where μ_0 is the "true" coefficient of friction, corresponding to the friction coefficient on a smooth surface, and θ is the slope angle of the asperity.

By performing a Fourier transform of the shear traces, it is clear that the oscillations present in the signal correspond closely to the average dome diameter ϕ (*cf.* Figure 3(b) and Figure 4(a); additional FFT of shear traces are given in the ESI in Figure S3). The magnitude of the peak, whose spatial frequency corresponds to the dome diameter, also increases with the applied load. This is evident in Figure 4(a) where the Fourier transforms of the shear traces obtained for the sample with an average dome diameter of $\phi = 175\,\text{nm}$ acquired at a velocity $v = 10\,\mu\text{m}\,\text{s}^{-1}$ at different loads are presented. Similar observations

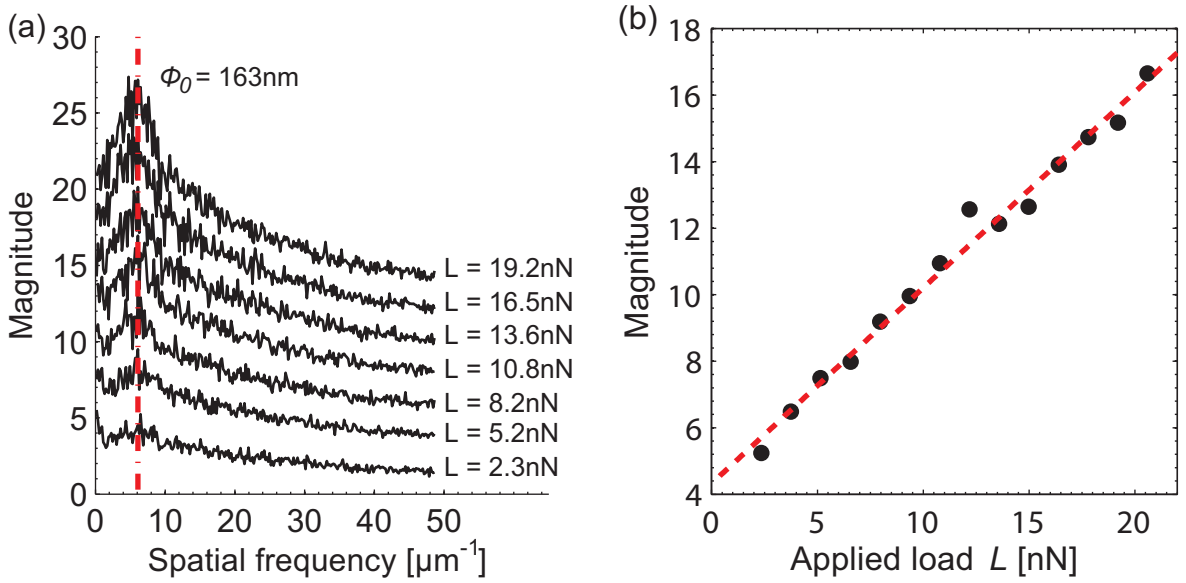

Figure 4: (a) 1D Fourier Transforms of the shear traces obtained for the $\phi = 175\,\mathrm{nm}$ nanodome textured surface at a velocity $v = 10\,\mu\mathrm{m\,s^{-1}}$. The curves are shifted vertically for clarity. A linear increase of the magnitude of the peak, whose spatial frequency corresponds to the average dome diameter, with the load L (b) is observed.

have also been made by Sundararajan *et al.*[42] on an AFM calibration grid consisting of 5 µm and 10 µm square pits. The direct topographic contributions consisted of localised lateral signal variations due to changes in surface elevation, resulting in peaks in the trace signal and valleys in the retrace signal. A similar behaviour was found at the microscale in a study where a silicon nitride ball attached to a tribometer was rubbed against a silicon sample with etched ridges of varying depths.[43,44] At a constant applied load, the presence of peaks in the friction signal corresponded to the spacing of the grooves. Thormann *et al.* also studied the characteristics of frictional shear traces on surfaces bearing vertically aligned micro-needles of 3 µm height spaced 5 µm apart using a silica colloidal probes of 7 µm and 32 µm in diameter. They noticed large oscillations in the shear signal, whose Fourier transform revealed a spatial frequency corresponding of the spacing between the micro-needles when the 7 µm probe was used. This called for a model in which both the climbing of asperities and the deformation of the needles should be taken into account.[16]

Furthermore, the magnitude of the peak corresponding to the average nanodome diam-

eter in the Fourier transform data magnitude increases linearly with the applied load L, as demonstrated in Figure 4(b). This means that the oscillations in the signal due to the presence of the nanotextures on the surface become more pronounced and well-defined as the applied load increases. The presence of such a well-defined peak is particularly noticeable at low scanning velocities. At high velocities, the tip might jump over a number of nanodomes during one stick-slip cycle. The samples with nanodomes of $\phi = 179\,\mathrm{nm}$ at velocities of $v = 1, 10$ and $100\,\mu\mathrm{m\,s^{-1}}$ (*cf.* Figure S3(g-i)) supports this argument, as the peak corresponding to the nanodome diameter becomes less defined as the velocity increases, with further peaks appearing at lower spatial frequencies (*i.e.* higher spacing) as the shear velocity increases.

Our observations of the stick-slip-like shear characteristics on nanodomed surfaces are thus consistent with previous studies,[16,19,37–39,42–44] in which the surfaces also bore textures or topographic features. It is also well established that stick-slip could occur at low shear velocities for lubricated surfaces.[45] However, due to the regularity of the nanotextures of our model surfaces, the occurrence of these frictional oscillations we have observed persisted through all the load and velocity regimes ($1\,\mu\mathrm{m\,s^{-1}}$ to $100\,\mu\mathrm{m\,s^{-1}}$) for all the nanodome sizes. That is, we did not observe smooth, kinetic sliding friction on the nanodome samples. Such sustained frictional instabilities are thus characteristic to the surface bearing well-defined nanotextures.

Friction-load relationship

A linear relationship between the applied external load and the resulting lateral force is observed for all samples in accordance with Amontons' first law of friction. It is important to note that due to the absence of smooth kinetic sliding, the lateral force f_s values were determined as half the difference between the average of the oscillations in the shear trace and retrace (*cf.* the blue lines in Figure 3). An example $f_s - L$ plot for the ϕ =92 nm dome sample at $0.5\,\mu\mathrm{m\,s^{-1}}$ shear velocity is shown in Figure 5, exhibiting a linear relationship for

both loading and unloading cycles. This relationship holds for all surfaces tested at shear velocities v ranging from $1\,\mu m\,s^{-1}$ to $100\,\mu m\,s^{-1}$. A finite friction force f_0 extrapolated at zero load can be attributed to the contributions by the adhesive force which can be considered as an effective load, as shown in the equation derived by Derjaguin:

$$f_s = f_0 + \mu L \tag{3}$$

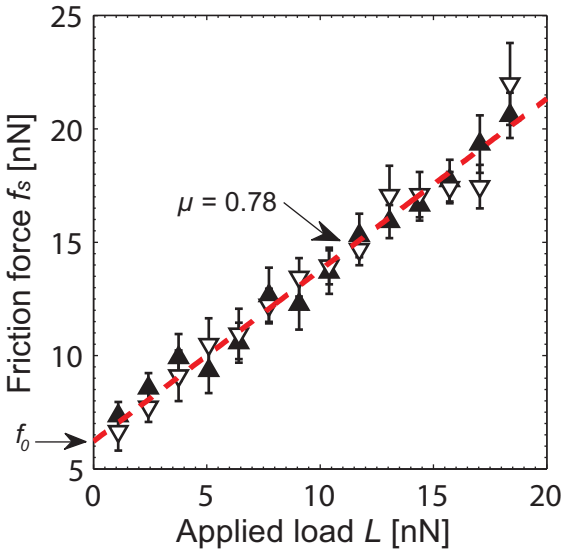

Figure 5: Linear dependence of the lateral force f_s on the applied load L, for the ϕ =92 nm nanodomed textured surface at v =0.5 $\mu m\,s^{-1}$ applied load velocity. The linear fit is for both loading (▲) and unloading (▽) cycles. The slope gives a friction coefficient of $\mu = 0.78$. The error bars represent the standard deviation from the mean of the shear traces. A finite friction force, f_0, is registered at the zero applied load as indicated by the arrow and is attributed to contributions from adhesion.

The apparent linear relationship between f_s and L exhibited here is consistent with previous frictional studies on nanostructured surfaces. For instance, such a behaviour has previously been reported by Pilkington *et al.*[19] on surfaces bearing nanoseeds, nanodiamonds, nanodomes and nanorods and in that study the linear relationship was discussed using various existing models. At the microscale, the linear nature of the friction-load relationship is commonly explained using models based on the Bowden and Tabor theory,[46] which states

that the real area of contact varies linearly with the applied load. The original model states that this relationship holds as long as the surfaces are plastically deformed. However, the inclusion of the Hertzian elastic deformation for multiple asperity contacts, complemented by the work of Greenwood and Williamson,[47] allows the retrieval of the linear relationship providing that the asperities have an exponential or Gaussian distribution of heights. At the atomic scale, where single asperity contacts are considered, explanations based on the *Tomlinson model*[30,31] and the *Cobblestone model*[48] have been used, with both models considering the energy dissipation as the result of climbing the asperities.

However, such a linear relationship between f_s and L has not always been observed for surfaces with nanotextures. In a previous AFM study, friction was measured between a 320 nm SiO_2 bead and porous anodic alumina films with pore sizes ranging from 31 nm to 372 nm. A non-linear dependence of the friction coefficient upon pore size was found, and this behaviour was explained by variations in the stick-slip effect which became more pronounced as the porosity and surface roughness of the sample increased.[18] The same conclusions were reached in another AFM study on friction between ordered (Ni) nanoporous membranes with pores of 270 nm and 370 nm and SiO_2 beads of 930 nm and 2280 nm in diameter.[49]

Whilst our results support the applicability of Amontons' first law to the nanodomed surfaces when we consider the average lateral force as the friction force, a common practice in AFM friction measurements, this is insufficient to fully characterise the shear characteristics of these nanotextured surfaces, which show pronounced and sustained frictional instabilities as discussed above.

Friction-topography relationship

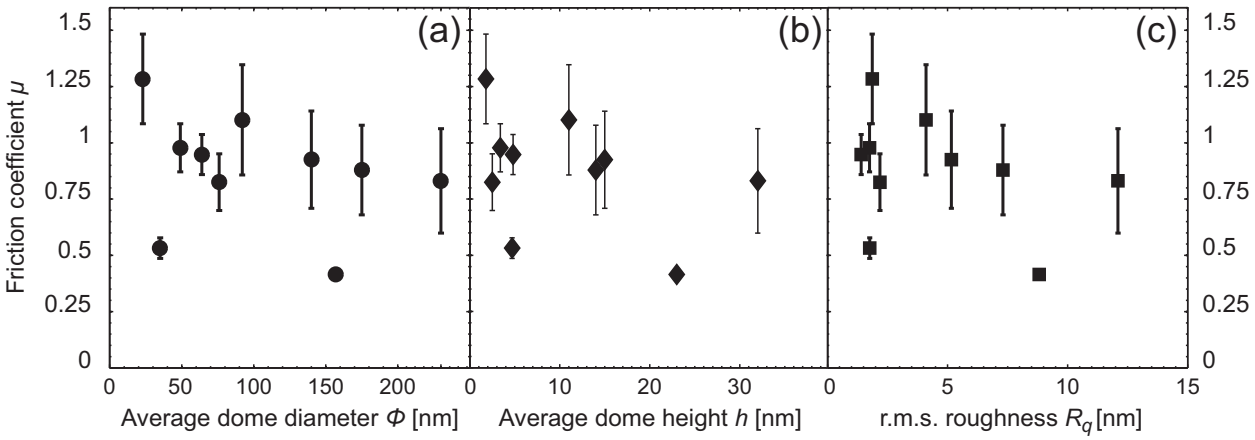

Figure 6: The variation of the friction coefficient μ with the average dome diameter ϕ (a), average dome height h (b) and r.m.s. roughness R_q (c) at a $10\,\mu m\,s^{-1}$ applied velocity, showing no correlation.

The friction coefficient μ of the samples is given by the slope of the friction *vs.* load curves (*cf.* Figure 5). The nanodomed surfaces may be considered as a convolution of the ubiquitous nanometre scale surface roughness superimposed on the domes of tens of nanometres in size. A number of previous studies have identified correlation between the surface topographic parameters and the friction coefficient. For instance, when studying the tribological behaviour of GeSbTe thin films, Bhushan and Koinkar found a linear correlation between the root mean square (r.m.s.) roughness of the samples and their resulting friction coefficient at loads greater than 140 nN, and explained this correlation using the *Ratchet mechanism*.[41,50] In our study, a lack of correlation is evident from the plot of the friction coefficient μ against the average dome size ϕ (average dome diameter), as shown in Figure 6 (a) at a shear velocity $v = 10\,\mu m\,s^{-1}$. Such lack of correlation is true for the data at all other shear velocities studied. Plotting μ against the dome average height h as shown in Figure 6 (b), or the roughness parameter *e.g.* r.m.s. roughness R_q (c) or average surface roughness R_a (not shown) does not reveal any trend either. More recently, Pilkington *et al.* also observed no direct correlation between the friction coefficient and these roughness parameters; instead they reported a correlation between the friction coefficient and a parameter defined as the

geometric friction coefficient μ_g. This μ_g was calculated by taking into account both lateral and vertical nano-features of the sample under investigation and the size of the AFM tip used during the experiments to include contributions to the friction coefficient from the average local slope of the nanotextures.[19] Although this correlation was not straightforward, it was observed that for all surfaces tested, the friction coefficient could be split into two parts, namely an intrinsic and geometric friction coefficient μ_0 and μ_g, the latter being defined as:

$$\mu_g \approx \frac{\delta}{d} \tag{4}$$

where δ and d are coefficients related to the vertical and lateral length scales, making μ_g a good representation of the average surface slope. δ can therefore be represented in our case as the r.m.s. roughness R_q or the average dome height h. The lateral length scale d takes into account the tip radius R and the average dome diameter ϕ and can be expressed as follows:

$$d \approx R + \frac{1}{2}\phi \tag{5}$$

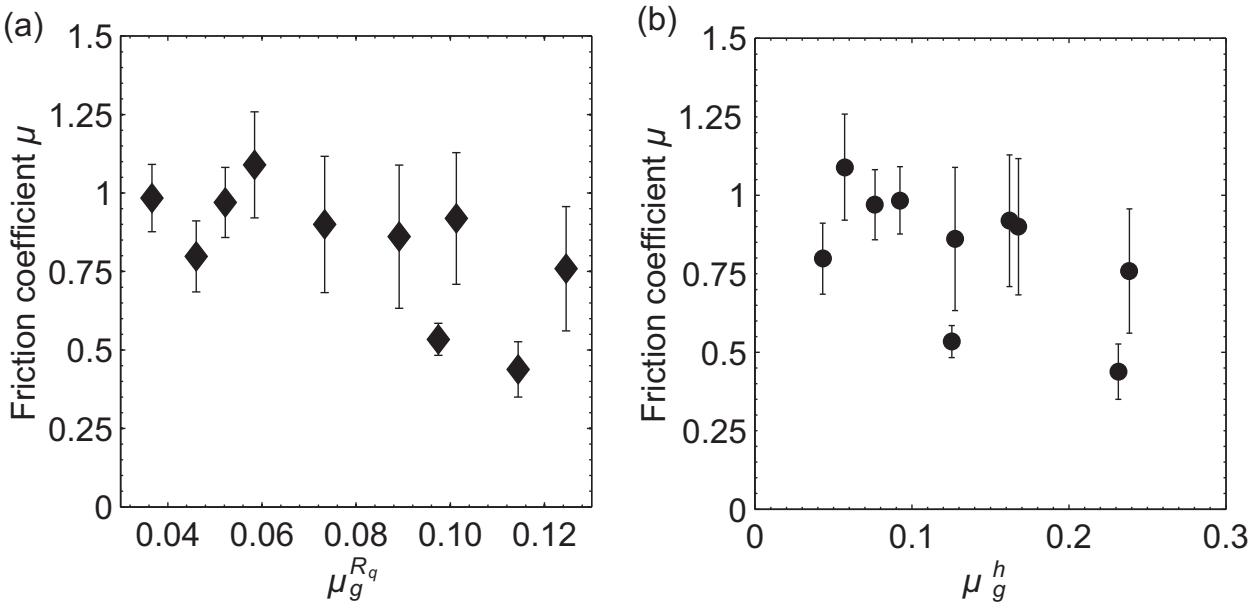

Figure 7: Variation of the friction coefficient, measured at a $v = 10\,\mu\mathrm{m\,s}^{-1}$ shear velocity, with respect to surface average local slope μ_g^i, where i is calculated using the the sample r.m.s. roughness R_q (a) and the average dome height h (b).

Once again, no correlation was found between the friction coefficient and these parameters (*cf.* Table S3 and Figure 7). A possible reason for this is that the friction encountered in our work results from the unstable sliding of the tip on the surface with no kinetic sliding.

One could argue that, although the dimension of the domes was systematically varied, the topographic geometry of the surface textures was retained, and thus the surface average slope did not vary greatly from sample to sample. However, we would like to relate to our discussion above, *i.e.* the shear characteristics of the nanodomed surfaces show sustained frictional instabilities with no kinetic frictional sliding observed. Thus, we suggest that the rationales and considerations proposed in previous studies, applicable to frictional sliding, cannot be readily applied to our results.

Contribution to friction by adhesion

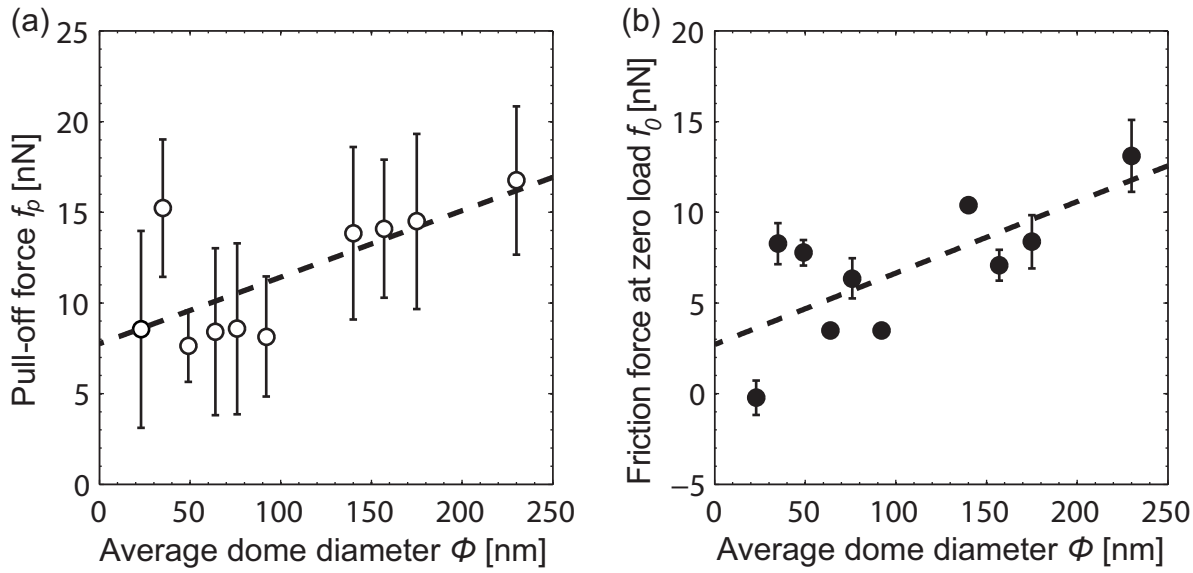

Figure 8: (a) Variation of the pull-off force, f_p, with nanodome average diameter ϕ. (b) Friction force at zero load, f_0, *vs.* ϕ. The dashed lines are a guide to the eye.

The contributions of the adhesive force as an effective load to overall friction are evident in Figure 5, where a finite friction force, f_0, is registered at zero applied load. The pull-off forces, related to adhesion, measured by taking a series of 18 force-distance curves, are plotted against the sample average dome diameter ϕ in Figure 8(a). There is a mild increase of f_p with ϕ. The adhesion between the AFM tip and the nanodomed surface is likely to arise from van der Waals forces and surface tension of bridging water menisci possibly present between the AFM tip and the surface; the latter is expected to dominate the measured adhesion or pull-off force, as the friction measurements were carried out in ambient conditions. Furthermore, the surfaces were UV-Ozone treated before the AFM measurement, rendering the surfaces hydrophilic.[51] It is also possible that menisci formed at the contacting asperities, giving rise to an attractive force due to the negative Laplace pressure inside the curved menisci. The large scatter in the data is due to the variation of the contact area, as the measurements were carried out at different contact spots, hence allowing the probe to land on top or in-between nanodomes. It is expected that the pull-off force measured would be lower if the

probe comes into contact with the surface on the apex of a dome rather than on a valley between domes. Similar positional variations in adhesion forces were found in a previous colloidal probe AFM study on structured rough surfaces, where a series of pull-off forces were acquired between a borosilicate glass sphere and a silicon calibration grid bearing triangular features.[52] Smaller pull-off values were registered when the contact spot was established on a single ridge as compared to when the contact was made with two ridges. In another AFM study where adhesion measurements were undertaken with a colloidal probe of 18 µm in diameter against a surface bearing 12 nm silica particles with different coverage densities (from 15 to 450 particles/µm^2), the pull-off forces measured were originally high for low coverage densities, then reached a minimum before increasing again slightly as the sample roughness increased, due to a change in contact area.[53] We thus ascribe the observed mild increase in the pull-off force with increasing dome diameter to the corresponding increase in the contact area. This interpretation is consistent with the observation of a mild increase in f_0, the friction force at zero applied load due to the adhesion contribution, as a function of dome diameter ϕ, as shown in Figure 8(b). However, as we have discussed above, the stick-slip-like shear characteristics cannot be explained by invoking the adhesion contributions and are related to the presence of nanotextures.

Effect of shear velocity on the friction coefficient

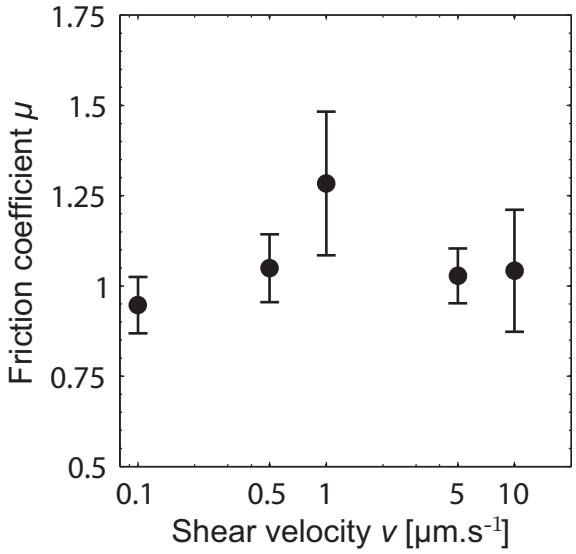

Figure 9: Velocity dependence of the friction coefficient on the shear velocity for the ϕ =23 nm nanodomed surface.

For all the dome sizes studied, our results reveal mild variations of the friction coefficient with velocity v within the error margin of the measurement, and ϕ *vs.* v plot for the sample of dome size $\phi = 23\,\mathrm{nm}$ is shown in Figure 9. The velocity dependence of friction has been the focus of numerous studies, and literature results on nanoscale friction measurements in ambient conditions have previously reported the velocity dependence of the friction coefficient ranging from a logarithmic increase, to a logarithmic decrease and to no dependence at all.[54] For example, a weak linear decrease was observed by Koinkar *et al.* on a flat Si(100) substrate over a velocity range from $400\,\mathrm{nm\,s^{-1}}$ to $400\,\mu\mathrm{m\,s^{-1}}$. Similarly, Pilkington *et al.* observed a weak decrease in the friction coefficient measured accross nanotextured surfaces with velocities ranging from $1\,\mu\mathrm{m\,s^{-1}}$ to $200\,\mu\mathrm{m\,s^{-1}}$, despite different characteristics of the shear traces of these surfaces.[19]

In a model developed to account for the velocity dependence of nanoscale friction,[55] the friction force is considered to arise from adhesion and the elastic deformation of the contacting asperities as well as the stick-slip behaviour. In the low velocity regime, the velocity

dependence may be explained using an extension of the *Prandtl-Tomlinson model* which takes into account thermal activation.[56] During a "stick phase", the probability for a thermally activated jump to occur would increase logarithmically as the velocity decreases, thus producing a logarithmic decrease of friction with the shearing velocity. A slight logarithmic decrease of friction was previously obtained in an FFM study on GeSbTe thin films of varied compositions and roughnesses[57] and was attributed to the kinetics of the capillary condensation water at the interface between the tip and the asperities. Such interpretations however remain qualitative as the detailed features of the tip are not always accurately known. If adhesion contribution dominates the total friction force,[54] we would expect a logarithmic decrease in friction with increasing shear velocity to track the decreasing number of menisci at the contacting interface. In our present case, the invariance of the friction coefficient with the sliding velocity is indicative of limited contributions to friction by adhesion. In addition, the shear velocity range tested may be insufficient to reveal the trends in different velocity regimes. For dry hydrophilic surfaces, a weak decrease of the friction force with the velocity has been reported within the range of velocities tested.[55]

Stick-slip frictional behaviour: the Stick-slip amplitude coefficient *SSAC*

In addition to the analysis of the applied load and velocity dependence on friction, the shear traces obtained were further analysed to account for the pronounced oscillations in the signal induced by the presence of the nanodomes on the surface (*cf.* Figure 3). These oscillations can be compared to a stick-slip frictional behaviour, and are in the present case attributed to the multiple collisions of the AFM probe with the topographic features of the surface, resulting in an unstable motion of the tip as it moves across the sample.

Previously, in an AFM study between an HOPG sample and an AFM tip in ultra-high vacuum conditions,[38] it was shown that the increase in the lateral force experienced by the AFM tip was due to an increase of the dissipative energy barrier, *i.e.* the *Schowoebel-Ehrlich*

barrier, at atomic step edges. This increased dissipation was convoluted to a topography-induced twist of the cantilever which resulted in a linear dependence between the lateral force experienced by the AFM cantilever and the applied load. This was later confirmed for other surfaces under ambient conditions and explained using a modified *Prandtl-Tomlinson* model which accounted for the tip-sample interaction at atomic surface steps.[58] When the stick-slip behaviour from AFM friction measurements is considered in this model, the AFM tip is postulated to get stuck in a potential energy minimum, resulting in an abrupt increase of the lateral deflection signal. The tip then remains in this position until enough energy is obtained for the tip to slide again, resulting in an abrupt increase of the lateral deflection signal. During this process, the energy is therefore rapidly dissipated, and the tip gets stuck again.

At the nanoscale, the variations of the friction shear traces have previously been attributed to a correlation with the local slope of the surfaces. In a study on rough molybdenum disulphide coatings, the shear data were analysed by decomposing the signal into two components, namely a constant value and a fluctuating one, the latter being dependent upon the variation of the local surface slope.[59] Fluctuations were also found in friction measurements on micro-grooved silicon surfaces at both micro- and nanoscale, where abrupt changes in topography led to sharp fluctuations in friction, hence an increase in the friction coefficient. In addition to this "slope" effect, it was also suggested that the collision of the tip with the asperities gave rise to an additional sharp peak in the signal as the tip's linear momentum was converted to angular momentum. It was also noted that the increase of the lateral signal could further be enhanced by an abrupt increase of the normal load due to the sudden lateral jump of the tip.[42]

In our study, the frictional signal consists of sharp peaks, suggesting that collisions between the tip and the nanodomes dominate. Indeed, the lateral shear signal exhibits an oscillatory period whose frequency approximately corresponds to the average dome diameter ϕ (*i.e.* the distance between two domes, as the domes are closely packed), as confirmed by

the 1D FFT of the shear traces (*cf.* Figure 3(b) and Figure 4(a)). Such instabilities, considered in our case mean that the contact between the AFM probe and the surface is largely disrupted, in contrast to the classic frictional sliding where constant contact is maintained. Atomic stick-slip is normally observed at low velocities only, whereas frictional instabilities on our nanodomed surfaces are exhibited over a velocity range spanning over two orders of magnitude.

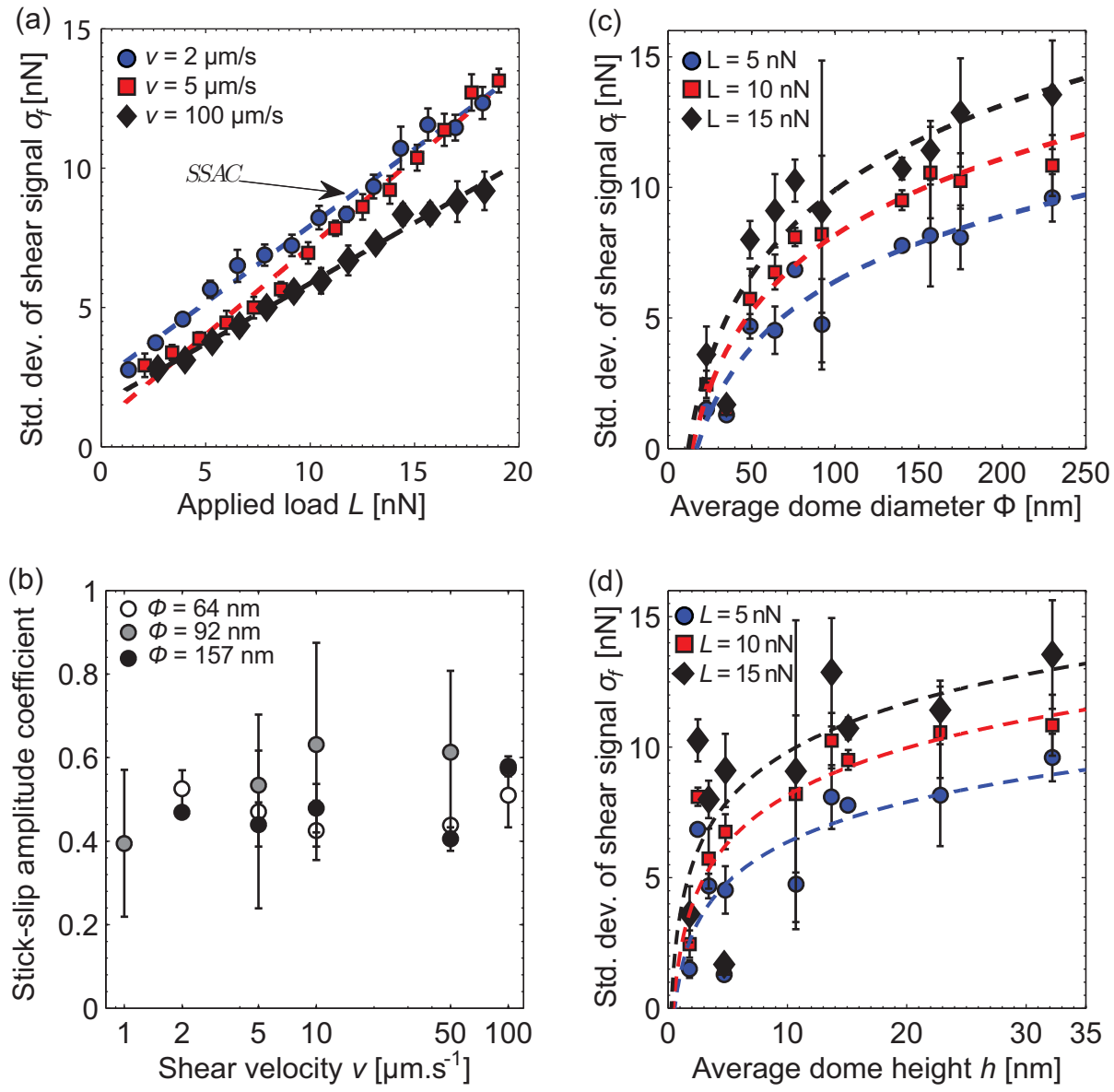

Figure 10: (a) Standard deviation of the shear signal, σ_f, *versus* the applied load L for the $\phi = 92\,\mathrm{nm}$ sample at a shear velocity $v = 2(\bullet), 5(\blacksquare)$ and $100\,\mu\mathrm{m\,s^{-1}}(\blacklozenge)$. The error bars represent the standard deviation of σ_f values. The slopes of the fitted curves are defined as the *stick-slip amplitude coefficient (SSAC)*. (b) Variation of *SSAC* with shear velocity for the samples bearing nanodomes with an average diameter of $\phi = 64(\circ)$, $92(\bullet)$ and 157 $\mathrm{nm}(\bullet)$. (c-d) Variation of σ_f under load $L = 5(\bullet), 10(\blacksquare)$ and $15\,\mathrm{nN}(\blacklozenge)$ at shear velocity $v = 10\,\mu\mathrm{m\,s^{-1}}$ against the average dome diameter, ϕ, (c) and the average dome height, h, (d). The dashed curves are logarithmic fits of the data points and a guide to the eye.

In order to characterise the magnitude of the instabilities encountered on our surfaces, we have examined the average of the standard deviation σ_f, averaged between the standard

deviation of the trace σ_t and the retrace σ_r, at each load. This amplitude parameter,σ_f, is plotted against the applied load L and shown for the $\phi = 92\,\mathrm{nm}$ in Figure 10(a) at 2, 5 and $100\,\mu\mathrm{m\,s^{-1}}$ velocities. It is clear from this plot that a linear relationship exists between the amplitude of the oscillations and the applied load. We define the slope of the linear trend as the *Stick-slip amplitude coefficient* ($SSAC$). Although the quantitative value of this coefficient also includes contributions from the feedback controller to the magnitude of the peak, the $SSAC$ has an important semi-quantitative meaning. It relates to the amplitude of the energy dissipated between an oscillation to the applied load. A similar (linear) trend was also reported by Meine *et al.*,[43,44] which was attributed to changes in the volume of sample elastically deformed when the probe hits a ridge.

In addition to the linear correlation between the amplitude of the oscillations and the applied load, a correlation has also been found between the sample topographic properties and the peak amplitudes, as shown in Figure 10(b) where the magnitude of the instabilities σ_f is plotted against the average dome diameter ϕ at applied loads of 5, 10 and 15 nN. All three plots exhibit a logarithmic increase of σ_f with the nanodome average diameter ϕ. This contrasts the lack of correlation between the friction coefficient μ and the sample topographic properties (*cf.* Figure S4). Given the approximately linear relationship between the dome height h and the dome diameter ϕ as shown in Figure 2(b), a similar correlation is also observed between σ_f and h, as shown in Figure 10(d). However, we do not observe a clear correlation between $SSAC$ and the shear velocity v, as evident from the $SSAC$ *vs.* v plots for the three samples, *i.e.* $\phi = 64, 92$ and $157nm$ in Figure 10(b).

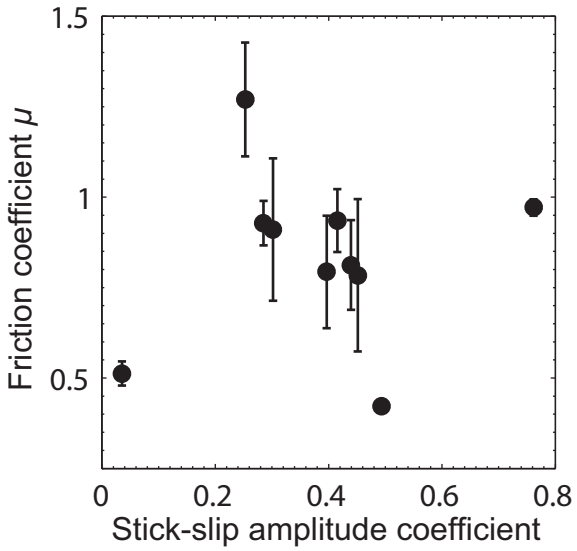

Figure 11: Variation of the Stick-slip amplitude coefficient ($SSAC$) against the surface friction coefficient.

In Figure 11, the friction coefficient of the nanotextured surfaces obtained at a velocity of $10\,\mu m\,s^{-1}$ is plotted against the stick-slip amplitude coefficient, and shows no explicit correlation. This suggests that the friction coefficient alone cannot provide a full description of the frictional behaviour of nanotextured surfaces where strong frictional instabilities are present. For example, a system could exhibit a low friction coefficient but with large frictional instabilities, *i.e.* with a large *Stick-slip amplitude coefficient* where sustained frictional instabilities dominate the overall frictional behaviour. This is of particular importance as most of the dissipated frictional energy is associated with energy instabilities, hence the SSAC parameter may serve as an indicator to wear properties of surfaces bearing nanodomes.

Conclusions

The frictional properties of surfaces bearing aluminium oxide nanodomes of well-defined geometry with features of various sizes were investigated by lateral force microscopy. The variation of the average lateral force was found to increase linearly with the applied load,

independently of the surface adhesion properties, in line with Amontons' first law of dry friction. Variations of the friction coefficient with shear velocity only revealed a weak dependence. No correlation was found between the friction coefficient and the surface topographic properties such as surface roughness and mean height of the nanodomes. The traces were found to be dominated by large oscillations due to frictional instabilities and the amplitude of the oscillations varied linearly with the applied load. We define the slope of this linear variation the "Stick-slip amplitude coefficient" ($SSAC$). Furthermore, it was found that the SSAC had no direct correlation with the friction coefficient, but is related to the surface topographic parameters. We propose that in the case of nanotextured surfaces, the friction coefficient may not allow a full description of the frictional properties, and that a description of the magnitude of the frictional instabilities should be considered for nanotextured surfaces.

Methods

Surface preparation

Full preparation details of the nanodomes textured surfaces are given in the Electronic Supplementary Information section (ESI). A short description of the preparation is summarised as follows. Aluminium oxide nanodomes were prepared by a two-step anodisation of aluminium foil (Alfa Aesar), carried out in oxalic or sulphuric acid electrolytes, with the final size of the domes dependent on the applied voltage.[60,61] Prior to the sample characterisation and friction measurements, the samples were cleaned with UV-Ozone (Jelight Company Inc, model 42A-220) treatment for 15 minutes.

Friction measurements

Friction measurements were performed using a Nanoscope Multimode III AFM equipped with a Picoforce controller (Veeco Instruments Ltd.), enabling closed-loop operation in the

normal direction. An uncoated, rectangular cantilever mounted with a tip of radius 10 nm was used (MikroMash CSC38-A, MikroMash, Estonia). Both normal and torsional spring constants were obtained by measuring normal and lateral resonance frequencies of the tip and the quality (Q) factors of the cantilever in air. These were then fitted, alongside with the cantilever's lateral dimensions (250 µm in length and 35 nm in width), to the hydrodynamic function for the normal (k_z)[62] and torsional (k_t)[63] spring constants, respectively. The normal photodetector sensitivity (δ_z) was obtained for each sample individually using the average slope of the compliance region on a series of 18 force-*versus*-distance curves. The lateral photodetector sensitivity (δ_t, in V/rad) was determined using the method of tilting the AFM head, as suggested by Petterson *et al.*[64]

Friction shear traces in both directions (*i.e.* trace and retrace, *cf.* Figure 3) were measured by monitoring the lateral deflection of the cantilever obtaining 5 × 1 µm scans (512 points per line × 16 lines), with the scanning direction set perpendicular to the long axis of the cantilever. The feedback gains were kept low during the scans to avoid feedback-induced oscillations of the cantilever.[65] The deflection setpoint was ramped up (*i.e.* increasing the load) to a maximum value of typically 3 V, and then down (*i.e.* decreasing the load) until the tip disengaged from the surface. The scanning velocity was also systematically varied from $v = 1$ to 100 µm s^{-1}. Each measurement was performed at two or more different locations on the sample. All measurements were conducted in air under controlled room temperature (21 ± 1 °C) and relative humidity (40 ± 10 % RH) conditions.

The data obtained were subsequently extracted in Matlab using an open-source software toolbox.[66] For each frame, the average and the standard deviation of each shear trace were then calculated after eliminating the first and last 25 points of each trace, so as to eliminate the instabilities encountered by the tip as its scanning direction was changed. The lateral deflection δV of the cantilever was taken as half of the difference between the trace and the retrace signals, and was further converted to the friction force as $f_s = \frac{\delta V \times k_t \times \delta_t}{h_{tip}}$, ($h_{tip} =$ 20 µm).[42] The adhesive pull-off force, *i.e.* the force necessary for the contact of the tip to

break the contact from the surface upon tip retraction, was also measured, and for each sample, 18 force-distance curves were made on a 3×3 grid at regular 1 µm intervals before and after the friction measurements. There was no evidence of plastic deformation of our nanodomed surfaces, as no evidence of wear was detected after the friction measurements.

Acknowledgement

W. Briscoe acknowledges funding from the Engineering and Physical Science Research Council (EPSRC; EP/H034862/1 and "Building Global Engagements in Research"), the Royal Society and the European Research Council (ERC), the European for Cooperation in Science and Technology (CMST COST) Action CM1101, and the Marie Curie Initial Training Network (MC-ITN) "NanoS3". E. Thormann and P. Claesson acknowledge support from the Swedish Foundation for Strategic Research program "Multi-functional pore arrays in silicon". B. Quignon is supported by a University of Bristol DTA studentship. Help from Andrew Collins (Bristol BCFN) is gratefully acknowledged.

Supporting Information Available: Electronic Supplementary Information: Sustained Frictional Instabilities on Nanodomed Surfaces: *Stick-Slip Amplitude Coefficient*. This material is available free of charge *via* http://pubs.acs.org.

Notes and References

1. Delrio, F. W.; de Boer, M. P.; Knapp, J. a.; Knapp, J. A.; David Reedy, E.; Clews, P. J.; Dunn, M. L. The Role of Van der Waals Forces in Adhesion of Micromachined Surfaces. *Nat. Mater.* **2005**, *4*, 629–634.

2. Mastrangelo, C. Adhesion-Related Failure Mechanisms in Micromechanical Devices. *Trib. Lett.* **1997**, *3*, 223–238.

3. Zhuang, Y. X.; Menon, A. On the Stiction of MEMS Materials. *Trib. Lett.* **2005**, *19*, 111–117.

4. Pilkington, G. A.; Briscoe, W. H. Nanofluids Mediating Surface Forces. *Adv. Colloid Interface Sci.* **2012**, *179*, 68 – 84.

5. Briscoe, W. H.; Titmuss, S.; Tiberg, F.; Thomas, R. K.; McGillivray, D. J.; Klein, J. Boundary Lubrication under Water. *Nature* **2006**, *444*, 191–194.

6. Chen, M.; Briscoe, W. H.; Armes, S. P.; Klein, J. Lubrication at Physiological Pressures by Polyzwitterionic Brushes. *Science* **2009**, *323*, 1698–1701.

7. Tseng, A. A.; Notargiacomo, A.; Chen, T. P. Nanofabrication by Scanning Probe Microscope Lithography: A Review. *J. Vac. Sci. Technol., B* **2005**, *23*, 877–894.

8. Biswas, A.; Bayer, I. S.; Biris, A. S.; Wang, T.; Dervishi, E.; Faupel, F. Advances in Top-Down and Bottom-Up Surface Nanofabrication: Techniques, Applications and Future Prospects. *Adv. Colloid Interface Sci.* **2012**, *170*, 2–27.

9. Bustillo, J. M.; Howe, R. T.; Muller, R. S. Surface Micromachining for Microelectromechanical Systems. *Proc. IEEE* **1998**, *86*, 1552–1574.

10. Zhai, T.; Yao, J. *One-Dimensional Nanostructures: Principles and Applications*; Wiley: New Jersey, USA, 2012.

11. Kim, H.-J.; Kim, D.-E. Nano-Scale Friction: A Review. *Int. Precis. Eng. Manuf.* **2009**, *10*, 141–151.

12. Ando, Y.; Ino, J. Friction and Pull-Off Force on Silicon Surface Modified by FIB. *Sens. Actuators, A* **1996**, *57*, 83–89.

13. Ando, Y.; Ino, J. Friction and Pull-Off Forces on Submicron-Size Asperities. *Wear* **1998**, *216*, 115–122.

14. Zhao, W.; Wang, L.; Xue, Q. Design and Fabrication of Nanopillar Patterned Au Textures for Improving Nanotribological Performance. *ACS Appl. Mater. Interfaces* **2010**, *2*, 788–794.

15. Yoon, E. S.; Singh, R. A.; Kong, H.; Kim, B.; Kim, D. H.; Jeong, H. E.; Suh, K. Y. Tribological Properties of Bio-Mimetic Nano-Patterned Polymeric Surfaces on Silicon Wafer. *Trib. Lett.* **2006**, *21*, 31–37.

16. Thormann, E.; Yun, S. H.; Claesson, P. M.; Linnros, J. Amontonian Friction Induced by Flexible Surface Features on Microstructured Silicon. *ACS Appl. Mater. Interfaces* **2011**, *3*, 3432–3439.

17. Zou, M.; Cai, L.; Wang, H. Adhesion and Friction Studies of a Nano-Textured Surface Produced by Spin Coating of Colloidal Silica Nanoparticle Solution. *Trib. Lett.* **2006**, *21*, 25–30.

18. Choi, D.; Kim, S.; Lee, S.; Kim, D.; Lee, K.; Park, H.; Hwang, W. Structure-Dependent Adhesion and Friction on Highly Ordered Metallic Nanopore Membranes. *Nanotechnology* **2008**, *19*, 145708.

19. Pilkington, G.; Thormann, E.; Claesson, P. M.; Fuge, G. M.; Fox, O. J. L.; Ashfold, M. N. R.; Leese, H.; Mattia, D.; Briscoe, W. H. Amontonian Frictional Behaviour of Nanostructured Surfaces. *Phys. Chem. Chem. Phys.* **2011**, *13*, 9318–9326.

20. Massi, F.; Berthier, Y.; Baillet, L. Contact Surface Topography and System Dynamics of Brake Squeal. *Wear* **2008**, *265*, 1784–1792.

21. Brace, W. F.; Byerlee, J. D. Stick-Slip as a Mechanism for Earthquakes. *Science* **1966**, *153*, 990–992.

22. Dieterich, J. H. Time-Dependent Friction in Rocks. *J. Geophys. Res.* **1972**, *77*, 3690–3697.

23. Dieterich, J. H. Time-Dependent Friction and the Mechanics of Stick-Slip. *Pure Appl. Geophys.* **1978**, *116*, 790–806.

24. Dieterich, J. H.; Kilgore, B. D. Direct Observation of Frictional Contacts: New Insights for State-Dependent Properties. *Pure Appl. Geophys.* **1994**, *143*, 283–302.

25. Dieterich, J. H.; Conrad, G. Effect of Humidity on Time- and Velocity-Dependent Friction in Rocks. *J. Geophys. Res.* **1984**, *89*, 4196–4202.

26. Ruina, A. Slip Instability and State Variable Friction Laws. *J. Geophys. Res.* **1983**, *88*, 10359–10370.

27. Scholz, C. H. Earthquakes and Friction Laws. *Nature* **1998**, *391*, 37–42.

28. Li, Q.; Tullis, T. E.; Goldsby, D.; Carpick, R. W. Frictional Ageing from Interfacial Bonding and the Origins of Rate and State Friction. *Nature* **2011**, *480*, 233–236.

29. Berman, A. D.; Ducker, W. A.; Israelachvili, J. N. Origin and Characterization of Different Stick-Slip Friction Mechanisms. *Langmuir* **1996**, *12*, 4559–4563.

30. Tomlinson, G. A. A Molecular Theory of Friction. *Philos. Mag.* **1929**, *7*, 905–939.

31. Socoliuc, A.; Bennewitz, R.; Gnecco, E.; Meyer, E. Transition from Stick-Slip to Continuous Sliding in Atomic Friction: Entering a New Regime of Ultralow Friction. *Phys. Rev. Lett.* **2004**, *92*, 134301–134304.

32. Tománek, D.; Zhong, W.; Thomas, H. Calculation of an Atomically Modulated Friction Force in Atomic-Force Microscopy. *Europhys. Lett.* **1991**, *15*, 887–892.

33. Hölscher, H.; Schirmeisen, A.; Schwarz, U. D. Principles of Atomic Friction: From Sticking Atoms to Superlubric Sliding. *Philos. Trans. Roy. Soc. London* **2008**, *366*, 1383–1404.

34. Xiangjun, Z.; Yonggang, M.; Shizhu, W. Nano/microtribology Stick-Slip Number under an Atomic Force Microscope and its Characteristics. *Tribology Letters* **2003**, *15*, 407–414.

35. Masuda, H.; Fukuda, K. Ordered Metal Nanohole Arrays Made by a Two-Step Replication of Honeycomb Structures of Anodic Alumina. *Science* **1995**, *268*, 1466–1468.

36. Ikegami, M.; Mie, Y.; Hirano, Y.; Suzuki, M.; Komatsu, Y. Size-Controlled Fabrication of Gold Nanodome Arrays and its Application to Enzyme Electrodes. *Colloids Surf., A* **2011**, *384*, 388–392.

37. Weilandt, E.; Menck, A.; Marti, O. Friction Studies at Steps with Friction Force Microscopy. *Surf. Interface Anal.* **1995**, *23*, 428–430.

38. Müller, T.; Lohrmann, M.; Kässer, T.; Marti, O.; Mlynek, J.; Krausch, G. Frictional Force Between a Sharp Asperity and a Surface Step. *Phys. Rev. Lett.* **1997**, *79*, 5066–5069.

39. Haugstad, G.; Gladfelter, W. L.; Weberg, E. B. Friction Force Microscopy of Silver Bromide Crystals: Ag0 Rods and Adsorbed Gelatin Films. *Langmuir* **1993**, *9*, 3717–3721.

40. Sung, I.-H.; Lee, H.-S.; Kim, D.-E. Prediction of Asperity Contact Condition using FFT-Based Analysis for Micro-Grooved Surface Design in Tribological Applications. *J. Phys. D: Appl. Phys.* **2003**, *36*, 939–945.

41. Bhushan, B. *Handbook of Micro/Nano Tribology, Second Edition*; CRC Press: USA, 2010.

42. Sundararajan, S.; Bhushan, B. Topography-Induced Contributions to Friction Forces Measured using an Atomic Force/Friction Force Microscope. *J. Appl. Phys.* **2000**, *88*, 4825–4831.

43. Meine, K.; Schneider, T.; Spaltmann, D.; Santner, E. The Influence of Roughness on Friction: Part I: The Influence of a Single Step. *Wear* **2002**, *253*, 725–732.

44. Meine, K.; Schneider, T.; Spaltmann, D.; Santner, E. The Influence of Roughness on Friction: Part II. The Influence of Multiple Steps. *Wear* **2002**, *253*, 733–738.

45. Drummond, C.; Israelachvili, J.; Richetti, P. Friction Between Two Weakly Adhering Boundary Lubricated Surfaces in Water. *Phys. Rev. E: Stat., Nonlinear, Soft Matter Phys.* **2003**, *67*, 066110–066126.

46. Bowden, F. P.; Tabor, D. In *The Friction and Lubrication of Solids*; Press, O., Ed.; Clarendon Press: United Kingdom, 1950.

47. Greenwood, J. A.; Williamson, J. B. P. Contact of Nominally Flat Surfaces. *Proc. Roy. Soc. London* **1966**, *295*, 300–319.

48. Israelachvili, J. N.; Chen, Y.-L.; Yoshizawa, H. Relationship between Adhesion and Friction Forces. *J. Adhes. Sci. Technol.* **1994**, *8*, 1231–1249.

49. Choi, D.; Lee, S.; Kim, S.; Lee, P.; Lee, K.; Park, H.; Hwang, W. Dependence of Adhesion and Friction on Porosity in Porous Anodic Alumina Films. *Scr. Mater.* **2008**, *58*, 870–873.

50. Koinkar, V. N.; Bhushan, B. Effect of Scan Size and Surface Roughness on Microscale Friction Measurements. *J. Appl. Phys.* **1997**, *81*, 2472–2479.

51. Shijian, L.; Wong, C. P. Effect of UV/ozone Treatment on Surface Tension and Adhesion in Electronic Packaging. *IEEE Trans. Comp. Packag. Technol.* **2001**, *24*, 43–49.

52. Tormoen, G. W.; Drelich, J.; Nalaskowski, J. A distribution of AFM Pull-Off Forces for Glass Microspheres on a Symmetrically Structured Rough Surface. *J. Adhes. Sci. Technol.* **2005**, *19*, 215–234.

53. Ramakrishna, S. N.; Nalam, P. C.; Clasohm, L. Y.; Spencer, N. D. Study of Adhesion and Friction Properties on a Nanoparticle Gradient Surface: Transition from JKR to DMT Contact Mechanics. *Langmuir* **2013**, *29*, 175–182.

54. Riedo, E.; Lévy, F.; Brune, H. Kinetics of Capillary Condensation in Nanoscopic Sliding Friction. *Phys. Rev. Lett.* **2002**, *88*, 185505–185509.

55. Nikhil, S. T.; Bhushan, B. Friction Model for the Velocity Dependence of Nanoscale Friction. *Nanotechnology* **2005**, *16*, 2309–2324.

56. Gnecco, E.; Bennewitz, R.; Gyalog, T.; Loppacher, C.; Bammerlin, M.; Meyer, E.; Güntherodt, H. J. Velocity Dependence of Atomic Friction. *Phys. Rev. Lett.* **2000**, *84*, 1172–1175.

57. Xie, G.; Ding, J.; Zheng, B.; Xue, W. Investigation of Adhesive and Frictional Behavior of GeSbTe Films with AFM/FFM. *Trib. Int.* **2009**, *42*, 183–189.

58. Hölscher, H.; Ebeling, D.; Schwarz, U. Friction at Atomic-Scale Surface Steps: Experiment and Theory. *Phys. Rev. Lett.* **2008**, *101*, 1–4.

59. Zhang Xiangjun, X.; Meng, Y.; Wen, S. Micro Contact and Stick-Slip Number Between AFM Probe Tip and Sample Surface. *Sci. China. Ser. E* **2003**, *46*, 537–545.

60. Mattia, D.; Rossi, M. P.; Kim, B. M.; Korneva, G.; Bau, H. H.; Gogotsi, Y. Effect of Graphitization on the Wettability and Electrical Conductivity of CVD-Carbon Nanotubes and Films. *J. Phys. Chem. B* **2006**, *110*, 9850–9855.

61. Leese, H.; Bhurtun, V.; Lee, K. P.; Mattia, D. Wetting Behaviour of Hydrophilic and Hydrophobic Nanostructured Porous Anodic Alumina. *Colloids Surf., A* **2013**, *420*, 53 – 58.

62. Sader, J. E.; Chon, J. W. M.; Mulvaney, P. Calibration of Rectangular Atomic Force Microscope Cantilevers. *Rev. Sci. Instrum.* **1999**, *70*, 3967–3969.

63. Green, C. P.; Lioe, H.; Cleveland, J. P.; Proksch, R.; Mulvaney, P.; Sader, J. E. Normal and Torsional Spring Constants of Atomic Force Microscope Cantilevers. *Rev. Sci. Instrum.* **2004**, *75*, 1988–1996.

64. Pettersson, T.; Nordgren, N.; Rutland, M. W.; Feiler, A. Comparison of Different Methods to Calibrate Torsional Spring Constant and Photodetector for Atomic Force Microscopy Friction Measurements in Air and Liquid. *Rev. Sci. Instrum.* **2007**, *78*, 93702–93710.

65. Schwarz, U. D.; Koster, P.; Wiesendanger, R. Quantitative Analysis of Lateral Force Microscopy Experiments. *Rev. Sci. Instrum.* **1996**, *67*, 2560–2567.

66. Carpick Lab's Software Toolbox (software tools for nanotribology research with AFM), http://nanoprobenetwork.org/software-library/welcome-to-the-carpick-labs-software-toolbox.